Modelling an Active Galactic Nuclei using a Neural Network

L. Castelli
L3 Computational Project, Computing Group C1
Submitted: March 12, 2021, Date of Experiment: 28.12.20-08.03.21

The aim of this project was to utilize the predictive power of a neural network in determining key components of active galactic nuclei. The QSOSED model was used to generate simulated spectral energy distributions, upon which three types of neural networks were trained and validated, before being tested on 29 real spectra. Validation revealed that a neural network was capable of learning a relation for accretion rate, returning a slope of 1.1 ± 0.1 between the predicted and actual values, which is in excellent agreement with the theoretical. A possible linear relationship is also noted for small distances; however, a linear relation was not appropriate when all distances were considered. No relationship is found for the predictions of the real active galactic nuclei parameters. We conclude that a neural network is able to learn a complex active galactic nuclei model, however further experimentation is needed to determine whether they can be applied to real active galactic nuclei or parameters other than accretion rate and distance.

I. INTRODUCTION

An active galactic nuclei (AGN) is a very bright accreting supermassive black hole at the center of a galaxy. AGNs are particularly luminous in the radio, ultraviolet and X-ray wavelengths. AGNs can be classified by their brightness relative to the galaxy they inhabit. A Seyfert is a very bright AGN with a clearly visible host galaxy. These Seyfert galaxies can be further split into Seyfert 1s and Seyfert 2s, based off of the width of their emission lines. A typical Seyfert 1 galaxy will have broad emission lines, indicating the presence of very fast moving gas above and nearby the accretion disk. If they also have narrow lines, they are called Narrow Line Seyfert 1 galaxies.

An accretion disk is formed when streams of material begin to orbit a black hole. The most basic description of these disks is the α-disk model, which assumes that the disk radiates as a blackbody. Gravitational pressure compresses the material into a plane parallel to the axis of rotation, until the internal thermal pressure rises enough to resist, forming a thin disk. A velocity gradient is present across the disk, with material nearer to the centre spinning faster than the material near to the edge. Therefore, the spinning material, primarily gas, experiences shear viscous forces. Inner material slows down, while outer material speeds up, leading to a net flow of mass inward and angular momentum outward [1]. A temperature gradient depending on radius is formed, with each annulus emitting as a blackbody according to:

$$F_\nu(T) = \frac{2h\nu\pi/c^2}{exp(h\nu/kT) - 1} \tag{1}$$

where ν and T are frequency and temperature respectively. All constants have their usual symbols. Summing over all the annuli, and over each frequency gives the total spectrum.

While AGN spectra resemble the form of the basic α-disk power law, there are additional features which need to be considered. Typically, there is a Kα iron line, as well as an additional component due to reflections. They usually also have a larger than expected flux density in the 0.3-2 keV range, coined the 'soft X-ray excess'. Another key component of the AGN spectra is the unexpected asymptotic behaviour at higher X-ray energies, known as the "hard X-ray tail'. While the fluorescent iron line and reflection components are typically attributed to hard X-rays reflecting off of the accretion disk, the soft X-ray excess and the hard X-ray tail are more complicated [2].

The hard X-ray tail can be solved with a optically thin, hot Compton zone [3]. This suggests that not all of the energy released via accretion is absorbed by the disk, but instead there exists an additional region in which photons are upscattered by relativistic electrons, and these high energy photons escape without being dissipated [4]. This region is usually considered to be the hot corona, an area of highly energetic particles near the blackhole.

The source of the soft X-ray excess is still unclear. Crummy et al. successfully fit this with a disk reflection model, using that the inner parts of the disk can be illuminated by emission from the previously discussed hot corona. Photoionization occurs, and the subsequent thermal radiation is blurred due to relativistic effects, leading to the excess [5]. Investigations into X-ray variability of AGNs further suggested a possible causality, as they found that fluctuations in the hard X-ray emissions, caused by the hot corona, were associated with delayed fluctuations in the soft excess [6]. However, later studies found that while reflection is at least partially responsible, it is not the major contributing factor [7].

The soft excess can also be fit by another Compton zone, one which is a warm and optically thick region [4]. The AGNSED model, produced by Done et al., combines the above observations into a single model. The area just past the inner most stable circular orbit (R_{ISCO}) is occupied by a corona, which acts as the hot, optically thin Compton region responsible for the hard X-ray tail [4]. This is followed by a truncated accretion disk, in which the outer region radiates as a blackbody like in (1), while the inner region acts as the warm, optically thick Compton zone [4]. This model has found success in reproducing AGN SEDs for a variety of blackhole types.

Machine learning has recently found success in classify-

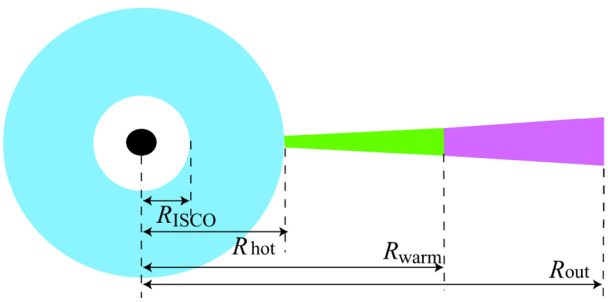

FIG. 1: Diagram of the AGNSED/QSOSED model from Fig.2a in Done et al. [4]. It has a hot and warm Compton zone (blue and green) and a standard blackbody disk (purple).

ing and modelling accreting blackholes [8] [9] [10]. Neural networks (NN) in particular have been used to decrease computation time for complicated spectral energy distribution (SEDs) modelling and have found better fits than modern methods [8] [10] [11]. This is largely due to its ability to approximate a wide range of functions and scaling performance with increasing data [12] [13].

In this paper, we attempt to train a NN to map from the X-ray spectral energy distribution (SED) of a bright soft X-ray AGN to six key features of an AGN: mass, spin, accretion rate, distance, inclination angle and redshift of a supermassive black hole, aiming to validate an NNs ability to learn a complex AGN model. If successful, the NNs will be used on 29 real AGN SEDs, to demonstrate whether they are able to generalize from a model to real world data.

II. METHODS

Grupe et al. put together a catalogue of 92 AGNs that had been observed by the SWIFT X-ray Telescope (XRT) and were both bright overall and bright in the soft X-ray [14]. In order to qualify, the AGN needed to be a Seyfert 1, have a negative hardness ratio (HR), a count rate of over 0.5 counts s^{-1}, and a galactic latitude of over 20 degrees. The HR is given by:

$$HR = \frac{H - S}{H + S} \tag{2}$$

where *H* is the number of counts between 0.5-2.4 keV and *S* is the counts between 0.1-0.4 keV [14]. Hence, a negative HR implies that the AGN is brighter in the soft X-ray than in the hard X-ray.

15 AGNs were originally selected from the catalogue to be used for testing and method validation, and their spectra were built using data and software from the UK Swift Science Data Centre [15]. Later, another 14 were selected to further investigate the results. For all observations, grades 0-12 were used, the XRT was in photon-counting mode and the SED was normalized, consistent with the process used by Grupe et al. [14]. The recommended single pass centroid method was used by the building software to further refine the coordinates of the source. As is standard for the XRT, the first 30 channels were ignored [15]. The energies, count rate per energy, exposure time, and errors of the spectrum were then extracted using XSPEC, an X-ray spectral fitting package [16].

The mass, redshift and accretion rate were all given in the catalogue, but the spin, inclination angle and distance were only available for a select few which had been studied in other papers. Where possible, these were found and included. See Appendix I for details.

The success of an NN scales with data [13]. To supplement the real SEDs, simulated data was generated according to the QSOSED model on XSPEC. QSOSED is a simplified version of the AGNSED model, and sets the electron temperatures, spectral indices, and radii of the two Compton zones as well as the outer radius of the entire disk to their standard values [15]. The six key parameters of the AGN listed previously are specified by user input, with the accretion rate, $\dot{m}$, being log scaled and converted to dimensionless units according to:

$$\dot{m} = \frac{\dot{M}}{\dot{M}_{Edd}} \tag{3}$$

In order for the simulated spectra to be comparable to the 30 AGNs, the six model inputs were chosen to be similar to those of a typical bright soft X-ray Seyfert 1 AGN.

Inclination angle can be constrained by noting the presence of broad emission lines in Seyfert 1 AGNs. As the relativistic gas capable of producing these lines is only present in the innermost region, the Seyfert 1s must not be observed through the ubiquitous dust and gas torus. Therefore, they must have a low inclination angle [5]. Hence we let the inclination angle only take small values less than 50°.

The spins of AGNs are typically also very high, as the large accretion disks increase angular momentum [5]. We therefore let the spin range between 0.5 and the model maximum of 1. The mass, accretion rate, redshift and counting time were taken to be the minimum and maximum of the 92 AGNs from the Grupe et al. catalogue and were respectively 2-450 $MM_{\odot}$, 0.02-2.45, 0.002-0.349 and 2-20 ks. It is noted that while super-Eddington accretion rates were allowed, $\dot{m}$ below 0.02 were not, and hence no advection-dominated accretion flow disks were included [4].

The distance was capped by the simulated detection limits of the XRT. Testing showed that few AGN were able to produce an observable spectrum beyond 6000 Mpc, and hence this was used as a maximum distance value. The minimum distance was determined by the smallest known distance in the catalogue, which was 65 Mpc for Mrk 355 [17].

Similarly, to make sure the SEDs had enough counts to remain above the detection limits, testing revealed that the total count rate per energy needed to be above 0.001 cts s^{-1} keV^{-1}. So, while the parameter space of mass, $\log \dot{m}$ and distance were equally sampled, any SED below this limit was discarded. To mimic the variance expected in real data, statistical noise is generated through assuming gaussian error, and is included appropriate to the observation time [16]. The simulated SEDs were also normalized, as with the real SEDs.

The QSOSED model required a response matrix (RMF) and an ancillary response matrix (ARF) for each simulation. These matrices describe how a piece of equipment processes a particular source and converts channel readings to energy readings. Data from Grupe et al. taken from before September 2007 used the RMF swxpc0to12s0_20010101v010.rmf, and afterwards used swxpc0to12s6_20010101v010.rmf [14]. To ensure both RMFs were represented, the simulations sampled them with equal probability. Grupe et al. created an ARF individually for each source, and hence the 15 ARFs associated with the original AGNs selected from the catalogue were randomly sampled for each simulation [14]. Each RMF and ARF was assigned a number, so that this information could be passed to the NN. 300,000 simulated SEDs were generated.

The simulated SEDs always produced 1000 energy – count pairs. The first 30 channels are removed, as in real SED analysis, corresponding to a loss of 5 pairs. However, 995 points is still far larger than the amount observed in the 15 real datasets, which fluctuated between 200 and 700 data points. Hence, the simulated SEDs were altered to be more comparable. A random number between 200 and 900 was chosen, and then pairs were culled randomly until the number of pairs matched the chosen number. This was done for every simulation thrice, producing 1,200,000 simulated SEDs.

The NNs were set up to take the all the basic information that is returned from an AGN SED in the form of a 1993

length list. The 995 energies in keV were followed by the 995 count rates per keV, then by the RMF and ARF number. The last element in the list was the counting time in seconds. For the real and altered data, the energy and rate lists were padded with 0s to match the necessary input length. The outputs were set to be the six key parameters listed before, each individually normalized. The inputs were passed through another normalization layer before processing to increase efficiency [13].

NNs consist of layers of neurons. The inputs are fed into each neuron and outputted according to:

$$A^{[l]} = g(W^l \cdot A^{[l-1]} + b^l) \tag{4}$$

where $A^{[l]}, W^{[l]}, b^{[l]}$ are the output, weight and bias matrices of layer *l*. These matrices are generated through vectorization, a technique which drastically decreases computation time [13]. The individual outputs, weights and biases from each neuron are concatenated to form three individual vectors, which are then stacked for each layer to create the three matrices. The next layer takes the results of the previous and repeats the above. The final layer produces the outputs $\hat{y}$, which are then compared to the actual value, *y*. *g* is a nonlinear activation function, for which we use the standard rectified linear unit as in Ribas et al., except for on the last layer, in which no activation function is used to allow the outputs to vary freely [10]. The performance of the network is evaluated using a cost function *J*, which describes overall how far off the predicted outputs are from the actual values:

$$J = \frac{1}{m}\sum_{i=1}^{m}(\hat{y}^{(i)} - y^{(i)})^2 + \frac{\lambda}{2m}\sum_{l=1}^{L}\|w^{[l]}\|^2 \tag{5}$$

where *m* is the number of inputs. The first summation in (5) makes up the bulk of *J*, and evaluates each prediction individually using a standard mean squared error function [15].

The second summation in (5) is from regularization. Networks can learn a given dataset to arbitrary accuracy, at the expense of not being able to generalize to unseen data. Therefore, we regularize the data, sacrificing predictive power for better generalization.

This is done through using L2 regularization and dropout layers [15]. L2 regularization is directly seen in (5), in which the L2 norm of every weight *w* in every layer *l* is squared and summed. The output of this sum is added to the cost, and hence a network is penalized for having large weights. The level of regularization is determined by λ, which is specified by user input. Dropout layers are added into the network itself and set a specified amount of a given layer's neuron outputs to 0. This forces a network to not rely overly on any one part. Both have been shown to improve generalization [13].

The network's weight and bias matrices are updated according to the cost function, and the performance is revaluated. This is done iteratively until the cost function fails to improve by more than 1% of the best value in 150 consecutive iterations. After completion, the cost at each iteration is plotted, and can be used to check for under or overfitting. Underfitting occurs when the model fails to fit the data enough and is solved through adding more neurons and layers. Overfitting occurs when the model becoming overly sensitive to the noise in the data. This sensitivity is reduced through regularization.

The parameters of the neural network, like the regularization constant λ, the number of layer and neurons per layer, were varied systematically to minimize the mean squared error in a validation set of 300 unseen simulated SEDs. Each network starts as only a single layer of 128 neurons and is adjusted using the plot of the cost function. After adjustment, the model is trained and checked again. This is continued until the mean squared error fails to improve by more than 1% of the previous lowest value. It is noted that due to computational constraints, no networks more than 6 layers, or layers with more than 2048 neurons were tested, as the testing time became prohibitive.

The 1% marker was used as a limit because after this point, in both the neural network parameter variation and the cost function minimization, testing revealed that further improvements had a negligble effect on the NN and its predictions.

To estimate the variance in the predictions of simulated data, 10 inputs are generated for each combination of parameters used. As the simulated SEDs have in-built noise, each will be slightly different and return different predictions. The mean and standard deviation of the predictions for these 10 inputs are calculated, from which the value and standard error are returned [18].

A similar method is taken to estimate the variance in the real data predictions, however instead of simply regenerating the spectra, the value and error on the count rate per energy is used to vary each point as a gaussian. This is done for every point in the spectra and repeated 10 times. The resulting 10 unique spectra are plugged into the NN. The variance in the predictions is once again used to return the standard error.

Three network types were used. The first network used the original dataset, before alteration, and was trained to demonstrate which parameters of the QSOSED model could be learned individually. The second network also used the original dataset but was trained to output all the parameters together. The third was used on the altered dataset, to create the best real data predictions for all of the parameters together. The network's predictions were plotted against the actual values and weighted linear and quadratic regression models were fit. The predictions for the 29 real AGNs were also plotted and fitted to regression models.

III. RESULTS

Network 1's individual accretion rate predictions performed best when using 2 layers composed of 512 and 256 neurons, which returned a mean squared error of 0.006. For the individual distance predictions using network 1 and the combined predictions from network 2, the best performance was achieved by using 3 layers composed of 1024, 512 and

Variable (Network)	Gradient	Y-intercept	χ^2_ν
$\log \dot{m}$ (1)	0.976 ± 0.006	0.005 ± 0.004	1.99
distance (1)	0.43 ± 0.02	0.0133 ± 0.0006	7.62
$\log \dot{m}$ (2)	0.865 ± 0.004	0.078 ± 0.001	3.05
distance (2)	0.61 ± 0.02	0.079 ± 0.007	9.22

TABLE I: Results of a weighted linear regression fitting to the predictions of $\log \dot{m}$ and distance from networks 1 and 2

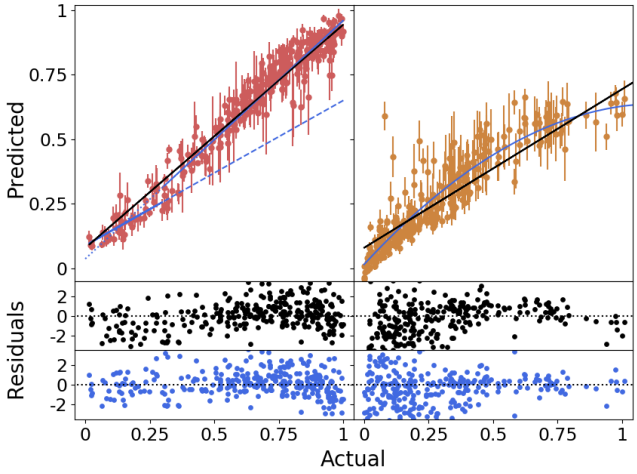

FIG. 2: Network 2's predictions vs actual values for accretion rate (red) and distance (orange) with a weighted linear (black) and split linear/quadratic (blue) regression model fit. Normalized residuals in the color of the regression model are included.

256 neurons, which returned a mean squared error of 0.014 and 0.056 respectively. The results of the weighted linear regression fittings are presented in Table I.

A possible secondary relationship was noticed for $\log \dot{m}$ less than 0.3 in the predictions from both networks. Weighted fittings of the values above and below 0.3 returned gradients of 1.01 +/- 0.01 and 0.89 +/- 0.04, with y-intercepts of -0.020 +/- 0.008 and 0.03 +/- 0.01 respectively for network 1. The separate linear models had a chi squared of 1.9 and 2.4 respectively. The split linear regression gradients were in excellent and mediocre agreement respectively with the theoretical gradient of 1 for a perfect model. The y-intercepts were both in mediocre agreement with the expected y-intercept of 0. The split for network 2 had gradients of 0.92 +/- 0.01 and 0.56 +/- 0.03, and y-intercepts of 0.037 +/- 0.008 and 0.088 +/- 0.001, with χ^2_ν = 2.9 and 1.6 respectively. These were not in agreement.

Inspection of the distance plots suggested that a quadratic model may be more appropriate, and so a weighted quadratic regression was fit to both the predictions of network 1 and network 2. For the results of network 2, a quadratic of form a = -0.47 $\pm$ 0.04, b = 1.08 $\pm$ 0.04 and c = 0.0146 $\pm$ 0.008 fit best with χ^2_ν = 4.2. For network 1, an unweighted regression fit better, producing a quadratic of form a = -0.47 $\pm$ 0.07, b = 1.10 $\pm$ 0.05, c = 0.011 $\pm$ 0.008 with χ^2_ν = 5.5.

For all parameters of network 3, and the other parameters of network 1 and 2, only the trivial relationship, in which the predictions do not vary with the actual values, was learned. The networks failed to achieve convergence.

For the real inputs, only accretion rate revealed any relation that was possibly different from the trivial, and a weighted and unweighted linear and quadratic regression model were fitted. An unweighted regression model for both model types returned a better fit with χ^2_ν = 6.9 and 6.8 respectively. The linear model had a gradient of -0.1 $\pm$ 0.4 and a y-intercept of 0.1 $\pm$ 0.4. The quadratic was of the form a = 0.4 $\pm$ 0.4, b = -0.7 $\pm$ 0.7 and c = -0.2 $\pm$ 0.2.

All errors are derived from the square rooted diagonals of the covariance matrices [18]. See detailed network architecture in Appendix II.

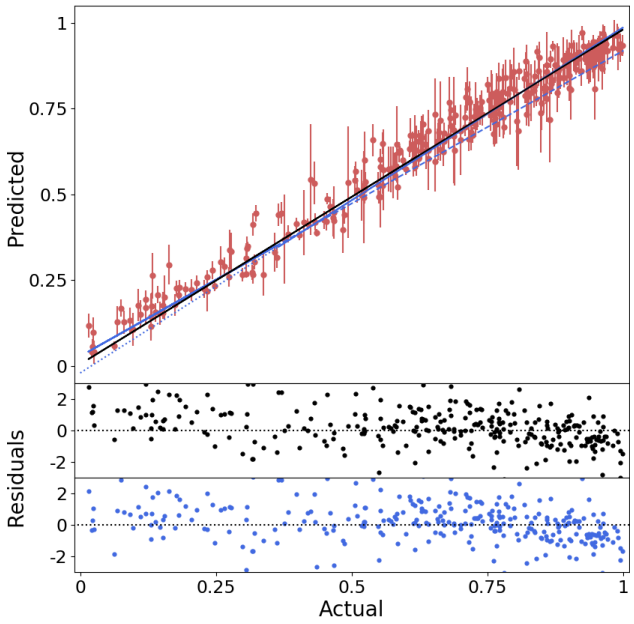

FIG. 3: Network 1's predictions vs actual values for $\log \dot{m}$ with a weighted linear (black) and a two part weighted linear (blue) regression fit. The unused parts of the two part linear regressions are dotted. Normalized residuals are in the color of the respective regression model used.

IV. DISCUSSION

For a perfect model, we expect a linear relationship between the predictions and the actual values with a gradient of 1 and a y-intercept of 0. Both of the standard linear regression models for the $\log \dot{m}$ predictions were not in agreement with the expected gradient. Furthermore, both showed a negative linear residual structure for values smaller than 0.3, and a large portion of the data is not within a single error bar. We therefore conclude that the original linear fits

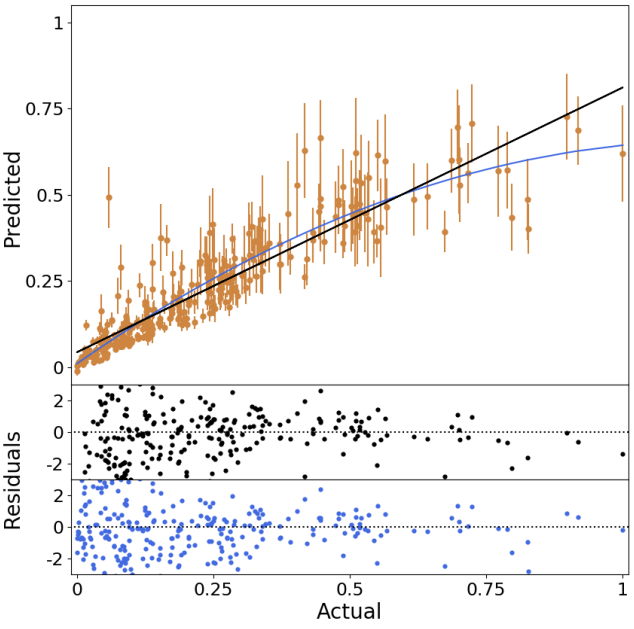

FIG. 4: Network 1's predictions vs actual values for dis tance with a weighted linear and quadratic regression fit. Normalized residuals are in the color of the respective regression model used

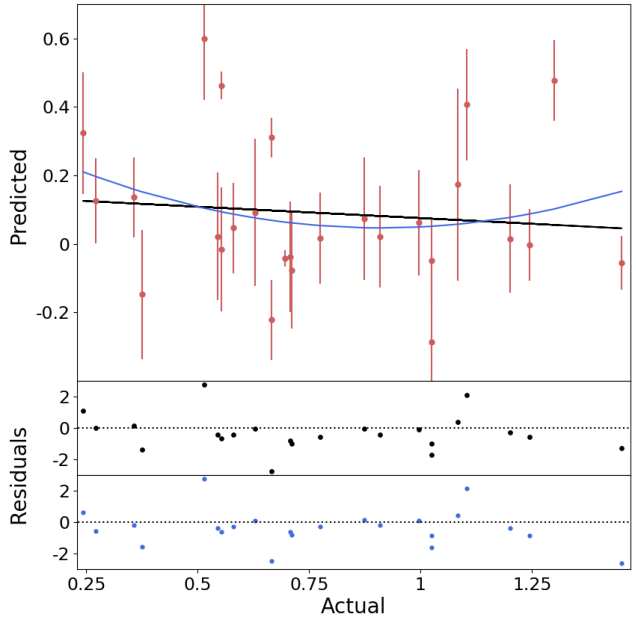

FIG. 5: Network 3's predictions vs actual values for accretion rate with an unweighted linear (black) and quadratic (blue) regression models fit. Normalized residuals are in the color of the respective regression model useds.

are not appropriate for the data.

A visual inspection of the two graphs supported the assertion that there may be a second linear relationship for values smaller than 0.3, which differed significantly from the linear relationship for values larger than 0.3. This is generally supported through fitting, which suggested that the χ^2_ν values were better than the original fits for three out of the four splits. It is noted that the one split for which the χ^2_ν is worse, the values less than 0.3 from network 1, this is largely due to the y-intercept being dragged down by two point at 0.1 and 0.3 with very small errors, and hence very large weights. These are likely outliers; however, the presence of multiple such points suggests a possible deeper systematic error, and hence they are not removed.

For the split linear regression fit from network 1, both linear models were found to be in agreement with the expected gradient and y-intercept. A visual inspection suggests that 2/3 of the data are within one error bar for the large $\log \dot{m}$ model, however only about 1/2 are for small $\log \dot{m}$. The χ^2_ν values were both relatively small, although for the lower $\log \dot{m}$ fit it is slightly larger. A downward turn is noted for $\log \dot{m}$ larger than 0.8 in the residuals, however it is relatively minor. We conclude that a linear relationship is appropriate for both models in the split, but that the linear relationship for the small model is clearly weaker and has more scatter.

The results for network 2 are similar, however instead the lower $\log \dot{m}$ fit is significantly better than that of the upper $\log \dot{m}$. The χ^2_ν is the best of any fit done with no clear residual structure, although again it has only about 1/2 of the data within one error bar. The upper $\log \dot{m}$ also has the downward turn residual structure noted above, but it is much more pronounced. Furthermore, the χ^2_ν is quite a bit larger, although around 2/3 of the data is within an error bar. A linear relationship is deemed appropriate for the smaller $\log \dot{m}$ fit, but the residual structure and large χ^2_ν suggest that for the larger $\log \dot{m}$ fit, a linear relationship is likely not appropriate.

For the two linear models fit to the predictions of distance, there is a significant inverted u-shape present in both residual plots. Additionally, for both fits more than half of the data is not within one error bar, and both have χ^2_ν values significantly larger than 1. We therefore conclude that a linear relationship is not appropriate for either network's distance predictions. The quadratic regression models fit the data better, and neither had any significant residual structure. However, while the χ^2_ν were both smaller than their linear counter parts, they were both still much larger than 1. Again, less than 2/3 of the data are within one error bar. Hence, we conclude that a quadratic regression is also not appropriate for the distance predictions.

The quadratic trend noted in the distance values may explain why the linear gradients for distance were so inaccurate. The larger distance values dragged down the linear regression, leading to the shallower gradient. Interestingly, the second term in both quadratic regressions, b, is within two standard errors of the expected gradient for a linear regression. This suggests that for the small values of distance, where the quadratic term can be ignored, there is a possible linear trend which is in reasonable agreement with our expectations.

While the lack of success on the parameters other than accretion rate and distance was disappointing, it was not unexpected. An X-ray SED is only a small part of an AGNs spectrum, and much of the information about an AGN is derived from examining the UV and optical bands, as well as other additional information. Spin and inclination angle are usually derived from examining Fe emission line smearing; however, line emissions are not considered in the QSOSED model. Redshift derivations use H1 maps of the universe [14]. Hence, this failure is not a surprise, as the NN was only provided with a small part of the data necessary to determine most of these values via modern methods.

However, the mass parameter clearly impacts the SED. In the AGNSED model, the coronal power emission was set to $0.02 L_{edd} \propto M$, and these emissions make up a large portion of the X-ray flux. Done et al. were able to fit real AGN SEDs by only varying mass and accretion rate, indicating that much of the spectrum is determined by only these two values (distance was not mentioned as it was already known) [4]. However, the model failed to learn this relation. It is suggested that while mass does have an effect, not having the accretion rate or distance known to the model makes it difficult for the NN to constrain, as a mass discrepancy can be mostly made up by changing the accretion or distance instead. This may explain some of the scatter observed as well as some of the large outliers discussed above, in which accretion rate/distance was adjusted to account for a variation in mass.

The above indicates one of the limitations of the end-to-end learning method used in these NNs. The lack of human guidance throughout the process can cause inefficiencies, preventing one from leveraging additional information and knowledge to perfect each step [20]. For large, complex networks these inefficiencies can cause the model not to converge, as was seen in network 3. For smaller networks like network 1 and 2, it fails to learn a relation which should exist, due to missing information about the other parameters.

It may also explain the deviations noted for small $\log \dot{m}$ and large distances, particularly when combined with the minimum total count rate per energy stipulation. Testing revealed that without a minimum count rate, very faint sim-

ulated AGNs were produced with large sections of the SED falling below detector limits. However, when this minimum is included, there is a selection bias. The parameter space of mass, $\log \dot{m}$ and distance are sampled equally, yet the combination must produce a bright AGN. So, if an AGN has a large distance or a small accretion rate, one or both of the other two parameters must be compensating. Without knowledge of the other parameters, the NN fails to account for this bias, causing predictions to become less accurate, potentially leading to the deviations seen.

The downward slope noted in the residuals starts occurring around the 0.8 mark, which corresponds to a $\dot{m} \geq 1$. This is consistent with a behaviour change discussed in Kubota & Done [19]. Specifically, they noted that the AGNSED (and hence by extension QSOSED) model could not fit super-Eddington AGNs, as the luminosity from the warm Compton region would be significantly reduced by advection effects to the point of being non-physical. This breakdown may explain the slight residual structure noted above for large accretion rates.

While the model was able to learn a relation for accretion rate in the simulated SEDs, it was not successful in learning a similar relation for real SEDs. For both fitted models, the χ^2_ν values were much larger than one and less than 2/3s of the data were within one error bar. While there aren't clear residual structures in either fit, it is likely that neither a linear nor a quadratic fit is appropriate for the data. However, even if there were a relation, all parameters in both fits are within one standard error of 0, indicating that the relation is not significantly different from the trivial relation discussed previously in Section III.

The NN failed entirely to generalize to real data. This is likely due to several factors. As discussed above, for $\log \dot{m}$ values greater than 0.8, the QSOSED model becomes no longer appropriate. Hence, the NN would be ill equipped to make predictions for any of the 11 super-Eddington AGNs tested. Another possibility is that the values the QSOSED model fixes, like the radii and electron temperatures of the Compton zones, are not appropriate for the real AGNs observed. Where Done et al. found success with their AGNSED model, they were able to constrain these values to better suit the AGN by using the optical and UV spectra [4].

The issue may not be constrained only to the NNs. The way in which the real accretion rates were calculated in Grupe et al. may have been partially at fault. The Eddington luminosity they used to predict accretion rate uses a mass scaling relation discovered in mass reverberation mapped galaxies [14]. However, very few AGN masses have been calculated yet via reverberation mapping, so Grupe et al. used a luminosity dependent method instead to calculate mass. The mass scaling relation may not hold for masses calculated via this other method, and hence could be another reason why the accretion rates did not agree with the predictions.

V. CONCLUSIONS

Three types of neural network are trained using AGN SEDs simulated according to the QSOSED model, and then applied to 29 real pieces of data. The SED, along with the exposure time, RMF and ARF types were fed into the network, and six key parameters of the blackhole were returned: the spin, redshift, and mass of the blackhole, along with its distance, accretion rate and inclination angle. The predictions of the NN were validated against the actual values for 300 simulated SEDs before the predictions and actual values for the real SEDs were compared.

The first two types of neural network, which were trained on the unaltered SEDs, returned a relation for both $\log \dot{m}$ and distance for the simulated data. A secondary linear relation was noted for $\log \dot{m} < 0.3$ in both models, and so two lines were fit to the $\log \dot{m}$ graph. We find that the gradients from network 1 for the $\log \dot{m}$ above and below 0.3 were in excellent and mediocre agreement with the theoretical. The cause of the secondary linear relation is attributed to the presence of selection bias. A downward turn was noted for $\dot{m} > 1$ and was thought to be caused by the QSOSED model breaking down due to advection effects.

For the distance predictions, a linear and quadratic model were both found to be inappropriate due to large scatter and residual structure. For small distances a possible linear relation in reasonable agreement with the theoretical was noted.

When applied to real data, no relationship was found between the predictions of the NN and the actual values for any of the six parameters. This is likely due to limitations of the QSOSED model, as well as possible discrepancies in the way in which the mass and $\log \dot{m}$ were calculated.

We conclude that a NN was able to learn a complicated theoretical model with moderate success, however, was unable to generalize to real data. Future research into the usage of NNs for interpreting SEDs, particularly the usage of multiple small NNs feeding into one another, is likely to be more successful with real data, as human input can be used to guide the network to more accurate predictions. It is possible that such work could potentially find the long sought-after method for determining distance from AGNs.

REFERENCES

[1] Raine D., et al., Accretion Processes in Astrophysics, 1998 (Cambridge University Press).
[2] Petrov, G., Mihova L., "AGN Spectra." Institute of Astronomy, 2005.
[3] Lubinski P., et al., MNRAS, 458, 2016, pp. 2454.
[4] Done C., Kubota A., MNRAS, 480, 2018, pp. 1247-1262.
[5] Crummy J., et al., MNRAS, 365, 2006, pp. 1067-1081.
[6] Fabian A. C., et al., MNRAS, 429, 2013, pp. 2917.
[7] Boissay R., et al., A&A, 588, 2016, A70.
[8] Chen B., et al., MNRAS, 501, 2021, pp. 3951-3961.
[9] Sreehar H., Nandi A., MNRAS, 502, 2021, pp. 1334-1343.
[10] Ribas A., et al., A&A, 642, 2020, A171.
[11] Silva L., et al., MNRAS, 410, 2011, pp. 2043-2056.
[12] Lu Z., et al., NIPS, 30, 2017, pp. 6232–6240.
[13] Ng A., Deep Learning Specialization, Coursera, 2019.
[14] Grupe D., et al., ApJ, 187, 2010, pp. 64-106.
[15] Evans P., et al., MNRAS, 397, 2009, pp. 1177-1201.
[16] Arnaud, K. A., in ASP Conf. Series, vol. 101, Astronomical Data Analysis Software and Systems V, ed. G. H. 1996. Jacoby & J. Barnes, 17
[17] Keek L., Ballantyne D., MNRAS, 456, 2016, pp. 2722-2734
[18] Hughes I., Hase T., Measurements and their Uncertainties, 2014 (Oxford University Press).
[19] Done C., Kubota A., MNRAS, 489, 2019, pp. 524-533.
[20] Glasmachers T., PMLR, 77, 2017, pp. 17-32.

APPENDIX I

The only AGN for which other values were found was MRK 355, in Keek & Ballantyne. They found that MRK 355 likely had a spin of 0.89 ± 0.89, a distance of 150.3 Mpc, and a inclination angle of 30° [17].

APPENDIX II

For network 1's accretion rate predictions, there were two dropout layers which dropped 0.2 and 0.1 of values respectively. λ was 0.0005. For network 1's distance predictions, there were three dropout layers which each dropped 0.1 of values respectively. λ was 0.0005. For network 2, there were also three dropout layers which each dropped 0.3 of values respectively. For network 3, the best result was achieved by 6 layers of 2048, 2048, 1024, 1024, 512, 256, each with dropout layers dropping 0.2 of all values. λ was 0.005.